Quantitative Review of Olivine Carbonation Kinetics: Reactivity Trends, Mechanistic Insights, and Research Frontiers

Quin R.S. Miller [1*], H. Todd Schaef [1], John P. Kaszuba [2, 3], Greeshma Gadikota [4], B. Peter McGrail [5], and Kevin M. Rosso [1]

[1] Physical and Computational Sciences Directorate, Pacific Northwest National Laboratory, Richland, Washington 99356, United States

[2] Department of Geology and Geophysics, University of Wyoming, Laramie, Wyoming 82072, United States

[3] School of Energy Resources, University of Wyoming, Laramie, Wyoming 82072, United States

[4] Department of Civil and Environmental Engineering, Cornell University, Ithaca, New York 14853, United States

[5] Energy and Environment Directorate, Pacific Northwest National Laboratory, Richland, Washington 99356, United States

Abstract

Magnesium-dominant olivine (Mg_2SiO_4) has received considerable attention for geologic and ex situ carbon mineralization due to its reaction potential with CO_2 and its abundance in mafic and ultramafic rocks. To enable better predictions and optimization of its carbonation rate, here we compile the results of 15 separate studies into an internally consistent kinetic framework. Time-dependent transformation curves were determined, analyzed, and used to calculate temperature-dependent carbonation rate constants between 50-300 °C. The unified results clearly show that olivine carbonation is optimized at 185-200 °C, and indicate a change in the carbonation reaction mechanism above 90 °C. Additional outcomes include the identification of important knowledge gaps and research frontiers for carbon mineralization, including those related to unraveling competitive serpentinization reactions, H_2O-saturated supercritical CO_2 (wet $scCO_2$) reactivity, and the formation and impacts of secondary surface coatings. In addition to supporting the deployment of carbon storage technologies in a climate-responding world, the findings may help improve understanding of how carbonation and serpentinization processes influence critical geochemical cycles.

Introduction and Background

Carbon capture and sequestration (CCS) is considered one of the most important technologies for mitigating the global temperature increase resulting from high concentrations of atmospheric CO_2.[1] Conventional CCS strategies are centered on capturing CO_2 and injecting it into deep saline sedimentary formations for long-term storage as a trapped fluid in the subsurface.[2, 3] However, injection of carbon dioxide into mafic and ultramafic rock is a favorable alternative due to abundant mineral- and glass-supplied divalent cations that can react in CO_2/H_2O fluids to form stable carbonate minerals, enabling relatively rapid permanent storage.[4-8] Recent field tests[9, 10] have successfully demonstrated carbonate mineralization due to injection of both supercritical CO_2 ($scCO_2$) and aqueous-dissolved CO_2 into continental basalt formations. Offshore storage within basaltic oceanic crust has also been proposed.[11, 12] And because of their extensive reaction potential[13-16], sub-seafloor and accreted ultramafic peridotites have been identified as promising targets for accelerated carbonation rates.[17]

Olivine, ranging from the magnesium-rich end-member forsterite (Mg_2SiO_4) to the iron-rich end-member fayalite (Fe_2SiO_4), is a primary source of carbonation potential within these host rock lithologies. In

particular, forsterite is a key constituent of upper mantle and lower crustal rocks. And given its relatively fast dissolution rate, forsterite has received considerable attention for geologic[18] and ex situ[19, 20] carbon mineralization by reaction with CO_2/H_2O fluids to form magnesium carbonates.

The overall forsterite carbonation reaction to form magnesite ($MgCO_3$) is (with the implied presence of H_2O and aqueous species):

$$Mg_2SiO_4 + 2CO_2 = 2MgCO_3 + SiO_2 \quad (1)$$

Depending on the reaction conditions, hydrated Mg-carbonates[21-23] may precipitate first (or instead of) anhydrous $MgCO_3$ due to sluggish Mg^{2+} dehydration kinetics[22, 24-29] that appears to cause an intrinsic energy barrier for direct crystallization of magnesite.[22, 30]

In competition with this reaction are parallel serpentinization reactions (hydration and oxidation) that consume dissolved magnesium, ferrous iron, and CO_2 species. Specifically, the production of hydrocarbons and Mg-bearing phases during serpentinization may reduce the carbonation yield. On the other hand, carbonate mineralization can also scavenge mobilized ferrous iron[31] and prevent it from being involved in redox reactions that generate hydrogen gas (H_2) and hydrocarbons (e.g., methane). The overall serpentinization reaction that describes the hydration of forsterite to form serpentine [$Mg_3Si_2O_5(OH)_4$] and brucite [$Mg(OH)_2$] is:

$$2Mg_2SiO_4 + 3H_2O = Mg_3Si_2O_5(OH)_4 + Mg(OH)_2 \quad (2)$$

Depending on the silica activity,[32] brucite dissolution may result in additional serpentine mineral precipitation:

$$3Mg(OH)_2 + 2SiO_2(aq) = Mg_3Si_2O_5(OH)_4 + H_2O \quad (3)$$

Unless it is first incorporated into brucite, serpentine, or carbonate phases, the oxidation of Fe^{2+} released from dissolving olivine may induce H_2 generation and magnetite (Fe_3O_4) precipitation:

$$12Fe^{2+} + 4H_2O = 4Fe_3O_4 + 3H_2 + 2H^+ \quad (4)$$

and this nascent magnetite may also catalyze further H_2 generation.[33] The H_2 can then participate in Fischer-Tropsch Type (FTT) reactions[34] of the general form:

$$(2n+1)H_2 + nCO_2 = C_nH_{(2n+2)} + nH_2O \quad (5)$$

including the Sabatier (methanation) reaction:

$$CO_2 + 4H_2 = CH_4 + 2H_2O \quad (6)$$

Given the complexity of these competitive reactions, among the collective body of related experimental work it remains unclear if a uniform kinetics 'signature' for forsterite carbonation is present that spans all conditions. In contrast to the olivine dissolution[35-37] and serpentinization[38-42] literature, where many of the results are typically presented with comparisons to previous work on similar systems, carbonation investigations to-date have largely been presented in the absence of quantitative kinetic comparisons from one study to the next.

The goal of the present review is to compile and compare the results of more than a dozen previous olivine carbonation studies on an equal footing. To do so we align the results of this body of work into a consistent kinetic framework, from which it then becomes possible to assess the prospect of predicting and/or co-optimizing carbonation-serpentinization reactions in natural or engineered settings. This approach is complementary yet distinct from review efforts[35-37] focused solely on olivine dissolution rates that don't

report carbonation kinetics and that cover relatively limited temperature ranges. A holistic understanding of coupled **Reaction 1** processes is important, as nucleation and growth of precipitating Mg-carbonate may control the overall rate of forsterite carbonation, depending on the temperature, fluid chemistry, mineralogical composition, reaction time, and occurrence and properties of secondary phases.[18, 43-47] The outcomes of this review include the identification of knowledge gaps and research frontiers for carbon mineralization, including those related to unraveling competitive serpentinization, H_2O-saturated CO_2 (wet $scCO_2$) reactivity, and the formation of secondary Si-rich surface coatings.

Carbonation Kinetics

Methods Overview

The forsterite reactivity literature was closely examined to identify investigations that evaluated carbonation in the experimental context of carbonate minerals produced and/or carbon consumed (**Table 1**). Experimental parameters and associated metadata, including time-dependent reaction extents, olivine composition and origin, and N_2 Brunauer–Emmett–Teller (BET) specific surface areas (SSA) of unreacted mineral powders were compiled from the text, tables, figures, captions, supplementary sections, and/or appendices of the publications. In some cases, information needed for the kinetic analyses was only available in figures, and a graphical analysis program[48] was used to digitize the data. The selected papers reported time-resolved olivine carbonation extents (or data that allowed the carbonation extent to be calculated), based on different methods, including in situ X-ray diffraction, in situ fluid sampling, or ex situ thermogravimetric carbonate quantification. The data from all studies were then assimilated into a consistent kinetics framework, here chosen to be the Avrami kinetic model[49], to calculate carbonation rate constants. The Avrami model, also known as the Johnson-Mehl-Avrami-Kolmogorov[50-52] model, is expressed as:

$$\alpha(t) = 1 - e^{-kt^n}$$

where α(t) is the reaction extent as a function of time (t), n is an empirical constant, and k is the rate constant.[53-57] This model is ideal for transformations with sigmoidal reaction profiles[58] and has been successfully applied to fluid-solid reactions[59], including carbonation[60, 61] and serpentinization kinetics.[40] The logarithmic transform of the Avrami equation was used to graph ln(-ln(1-α)) vs. ln(t), in which the rate constant, ln(k), is the y-intercept, and n is the slope of the least-squares line of best fit through the plotted data points.[56] The dimensionless exponent, n, potentially provides insight into the time-dependence and dimensionality of nucleation and growth processes, especially for strictly solid-state transformations.[53, 58, 62] Although n is dependent on the reaction mechanism(s)[49, 63-69], including temperature-dependent mechanisms[56, 61, 64, 70-72], specific physical significance of Avrami exponents, generally, remains questionable[73-75], and subsequent literal interpretation[53] of n for hydrothermal nucleation and growth should be viewed cautiously. The calculated Avrami parameters and uncertainties are listed in **Table S1**.

Time-Transformation Relationships

Reaction profiles that display time-resolved carbonation extents from the compiled studies[27, 29, 41, 76-86] are shown in **Figure 1**. For clarity, the datasets were organized into two groups according to the methods for calculating reaction extent **(Table S1)**. **Figure 1a** shows time-transformation relationships for which the reaction extent has been determined by in situ or ex situ measurements of precipitated carbonate minerals, where total consumption of the olivine present represents 100% reaction. Time-resolved reaction extents reported in **Figure 1b** are based on analyses of carbon in the fluid, where reaction extent is calculated based on consumption of the initial CO_2 present in the experiment (13.7-360 mmol/kg, **Table 1**). All of the studies investigated olivine with at least 87% of the divalent metal sites occupied with Mg^{2+} (Fo_{87},

$Mg_{1.74}Fe_{0.26}SiO_4$). The samples were either synthesized (nominally Fo_{100}) or sourced from four distinct locales (**Table 1**). Most of the analyzed datasets evaluated, by design, only carbonation, but the experimental conditions of seven studies[41, 77-80, 83, 85] examined both carbonation and serpentinization reactions. Deriving insight from direct comparisons of time-transformation trends for these collected studies is difficult due to their diverse experimental parameters, including olivine composition, grain sizes, SSA, water-rock ratios, pressure, pH, dissolved carbon, water activity, and CO_2-H_2O fluid ratios. One salient insight from **Figure 1** is that experiments containing an immiscible $scCO_2$ fluid (**Table 1**), and therefore bicarbonate availability in constant excess, resulted in faster carbonation, as they were farther from equilibrium relative to experiments that contained limited dissolved carbon. Although some assessments are possible solely through analysis of time-transformation profiles, unification of the various datasets into the kinetic model is required for more meaningful interpretations.

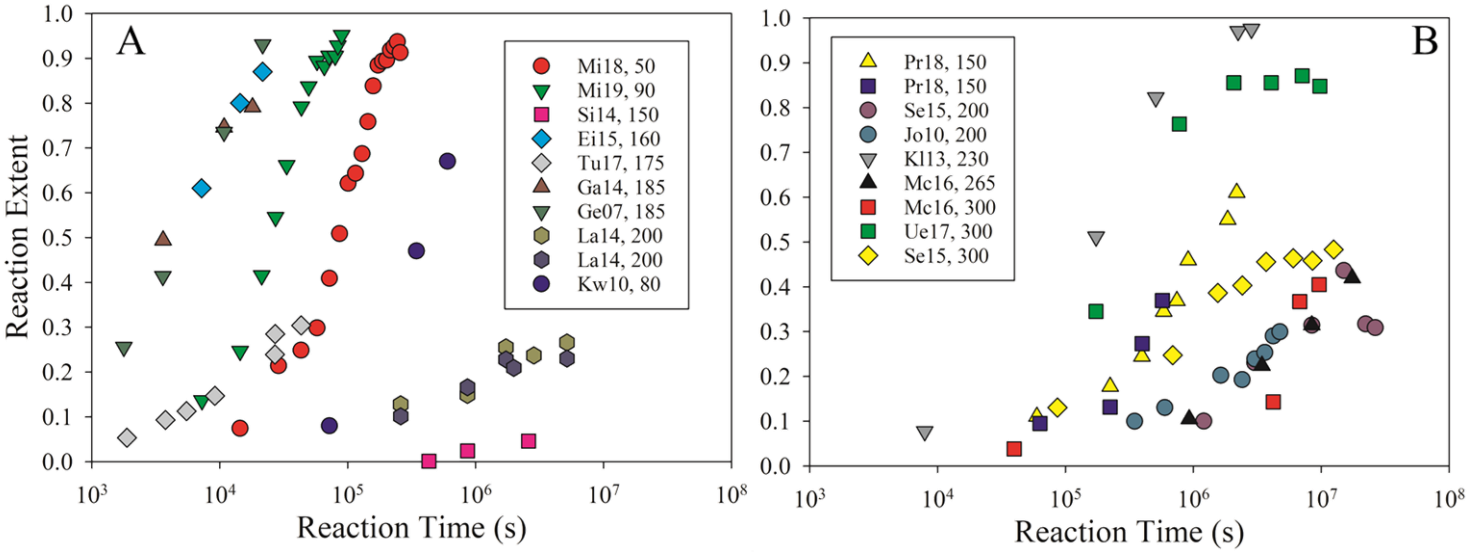

Figure 1. Time-transformation results from analyzed olivine carbonation datasets [27, 29, 41, 76-87] that show carbonation extent as a function of time. As described in the text, Panel A reaction extents were determined by *in situ* or *ex situ* measurements of precipitated carbonate minerals, and Panel B reaction extents are based on analyses of carbon in the fluid. Except for La14[77], Panel A studies were conducted under conditions in which a separate $scCO_2$ phase was present, while the remaining studies were conducted with a finite quantity of dissolved carbon. Abbreviations correspond to the first two letters of the first author's name, are followed by the last two numbers of the publication year (**Table 1**), and the additional number corresponds to the experiment temperature (°C).

Table 1. Selected experimental parameters for compiled studies[27, 29, 41, 76-87] shown in **Figure 1**. More experimental details listed in **Table S1**.

Study (Figure 1a)	Abbreviation	Temperature (°C)	Olivine Composition (Fo#)	Olivine Type	N_2 BET SSA (m^2/g)	Particle Size Range (µm)	CO_2 Pressure (bar)	$NaHCO_3$ (M)	NaCl (M)	W/R	in situ pH / benchtop pH
Miller et al. 2018[27]	Mi18	50	100	SF	26.7	0.031*	90	-	-	2.2	- / -
Kwak et al. 2010[87]	Kw10	80	99	SF	1.0	-	97	-	-	1.0	- / -
Miller et al. 2019[29]	Mi19	90	100	SF	26.7	0.031*	90	-	-	2.2	- / -
Sissmann et al. 2014[86]	Si14	150	88	SC	0.13	33-80	280	-	-	10.0	3.2 / -
Eikeland 2015[82]	Ei15	160	93	NO	-	<10	100	0.5	0.5	5.0	- / -
Turri et al. 2017[84]	Tu17	175	93	NO	-	70-250	100	0.64	1.0	2-3	- / -
Gadikota et al. 2014[81]	Ga14	185	87	TS	3.77	<75, 21.4**	141	0.64	1.0	6.7	6.4 / -
Gerdemann et al. 2007[76]	Ge07	185	87	TS	-	<75, 21.4**	152	0.64	-	5.7	- / -
Lafay et al. 2014[77]	La14	200	91	SC	2.3	<30	-	1.0	-	15	- / 8.9
Study (Figure 1b)	**Abbreviation**	**Temperature (°C)**	**Olivine Composition (Fo#)**	**Olivine Type**	**N_2 BET SSA (m^2/g)**	**Particle Size Range (µm)**	**Pressure (bar)**	**$\sum CO_2$ (mmol/kg)**	**NaCl (M)**	**W/R**	**in situ pH / benchtop pH**
Prikryl et al. 2018[80]	Pr18	150	90-94	NO	-	45-125	4.7	5.17-20.9	0.011-0.03	8.0	- / 6.5
Sekine et al. 2015[85]	Se15	200, 300	90	SC	-	10-200	400	360	-***	4.0	9.3 / 10
Jones et al. 2010[78]	Jo10	200	88	CN	0.929	100	300	90	0.5	2.5	6.8 / 9.4
Klein and McCollom 2013[79]	Kl13	230	91	SC	0.59	53-212	350	209	0.5	2.3	5.4 / 6.3
McCollom et al. 2016[41]	Mc16	265, 300	91	SC	0.59	53-212	350	~21	0.5	2.1-2.6	8-8.4 / 7.8-8.4
Ueda et al. 2017[83]	Ue17	300	90-91	SC	-	>100	500	65	0.55	5.0	- / 5.9

*average crystallite size determined by X-ray diffraction
**mean grain size of the Ge07 sample determined by Ga14
***The Se15 experimental fluids contained 1100 mmol/kg of NH_3.
Abbreviations: -, not reported and/or not applicable; SF, synthetic forsterite; SC, San Carlos (CA, USA); TS, Twin Sisters (OR, USA);NO, Norway; CN, Canada; BET SSA, Brunauer–Emmett–Teller specific surface area; W/R, water-rock ratio; Fo#, percent of divalent metal sites occupied by Mg

Avrami Rate Constants and Mechanistic Insights

The Avrami rate constants and associated N_2 BET SSA-normalized rate constants for olivine carbonation from the compiled studies[27, 29, 41, 76-86] are shown in **Figure 2**. The temperature-dependent trends for carbonation rate constants are relatively well-defined, considering the wide range of experimental conditions. Due to the initial reaction inhibition (see *Si-rich Surface Layers* discussion and **Table S1**) in Sissmann et al.[86], we removed the five-day induction time (c.f., Croker et al.[71] and Vu et al.[69]). The caveat of this approach is that only two datapoints remained, precluding calculation of model uncertainties (**Figure 2** and **Figure 3**). Overall, the Avrami rate constants (**Figure 2a**) and BET SSA-normalized rate constants (**Figure 2b**) produced strikingly consistent trends in measured olivine carbonation kinetics. The initial Albany Research Center (ARC) U.S. Department of Energy reports[88, 89] and the subsequent publication[76] used isotemporal experiments to identify 185 °C as the optimum olivine carbonation temperature, confirmed by Chizmeshya et al.[90] **Figure 2** clarified that the most rapid olivine carbonation occurs at ~185-200 °C, again confirming the ARC results. Their carbonation extent data[88] is also plotted in **Figure 2b** to facilitate an (indirect) comparison of reaction trend morphologies. The temperature dependence trends for olivine carbonation kinetics are qualitatively consistent with other previous experimental work, as carbonation of simulated ultramafic mine tailings from 200-300 °C was optimized at 250 °C.[91] Similarly, carbonation of olivine was found to be slower at 500 °C compared to 400 °C [92], and rhyolite alteration by CO_2-rich water was faster at 200 °C compared to 350 °C. These trends are all likely due to reduced extents of carbonic acid dissociation at higher temperatures[93] and the onset of magnesite thermal decomposition.[23, 27]

The temperature trends in **Figure 2** are suggestive of parallel carbonation (**Reaction 1)** and serpentinization (**Reactions 2-6**). The 300 °C carbonation rate constants are likely artificially elevated, as the calculation of carbonation rate is overprinted with serpentinization reactions, whose rates and products are unconstrained. Carbonation rates therefore only appear to be elevated at 300 °C, as CO_2 could be consumed by brucite carbonation[94, 95] and/or transformation to graphite[92, 96], organic acids[97], and hydrocarbons[98] (**Reactions 5-6**). Furthermore, the uppermost 300 °C rate constant is from a study[85] in which olivine of unknown SSA was reacted with ammonia (NH_3)-rich solutions (1100 mmol/kg). The influence of NH_3 on olivine carbonation and serpentinization is currently unclear, though ongoing work[99] should provide insight into this question.

Plotting the Avrami exponents (**Table S1**) as a function of temperature enables some new mechanistic insight into the carbonation process to be obtained (**Figure 3**). If only the studies shown in **Figure 1a** are considered in **Figure 3**, the exponent appears to decrease between 50-200 °C. However, the compiled Avrami exponents remained essentially constant for two temperature ranges, suggestive of a bimodal distribution. Between 50-90 °C, n is ~1.24, and between 150-300 °C, n is ~0.52. Exponent trends for **Table 1** studies are uniformly suggestive of a change in forsterite carbonation mechanism between 90 and 150 °C. We suggest that the change in n **(Figure 3)** can be attributed to a change in the carbonate growth mechanism. Although further work would be required to understand the basis for this change at the molecular level, Saldi et al.[100], using hydrothermal atomic force microscopy between 80-105 °C, identified a change in the growth mechanism of magnesite below 90 °C; the growth rate at low temperatures was controlled by step advancement rates, while at higher temperatures it was controlled by step generation. Our kinetic analysis, while being unable to confirm or refute this hypothesis without additional nanoscale experimental work (c.f., Lüttge[101]), is nonetheless consistent with the Saldi et al.[100] mechanistic interpretation, and extends the relevant temperature range to 50-300 °C. The slower process of step advancement[100] likely contributes to slower overall olivine carbonation rates at 90 °C,[47] and provides a rational basis to explain why the observed rates are temperature-dependent. It is noteworthy that temperature-dependent olivine dissolution kinetics

don't appear to have discontinuities between 22-150 °C[35, 37], highlighting the importance of quantitatively examining coupled dissolution-precipitation reactions.

Knowledge Gaps and Research Frontiers

Competitive Serpentinization Processes

Our kinetic analysis provides a basis for focusing future work on key unknowns that could improve understanding of transformation kinetics in the subsurface and aid in the development of various CCS technologies. For example, the potential for concomitant carbon mineralization and H_2 production is intriguing, as together they may contribute to negative-emissions hydrogen utilization.[102] The possibility for coupling olivine carbonation with serpentinization-derived H_2 production in an industrially-relevant process has been discussed by investigators[39, 42], who explored Al-catalyzed olivine hydration. Other workers have experimentally investigated H_2 generation and carbon capture from industrial wastes via the hydrothermal alteration of steel slags[103] and simulated mafic mine tailings.[91] It is possible that controlling the reaction temperature in ex situ or enhanced geologic processes will help co-optimize carbon mineralization and H_2 generation, as serpentinization rates are optimized at 280-310 °C[40, 104, 105].

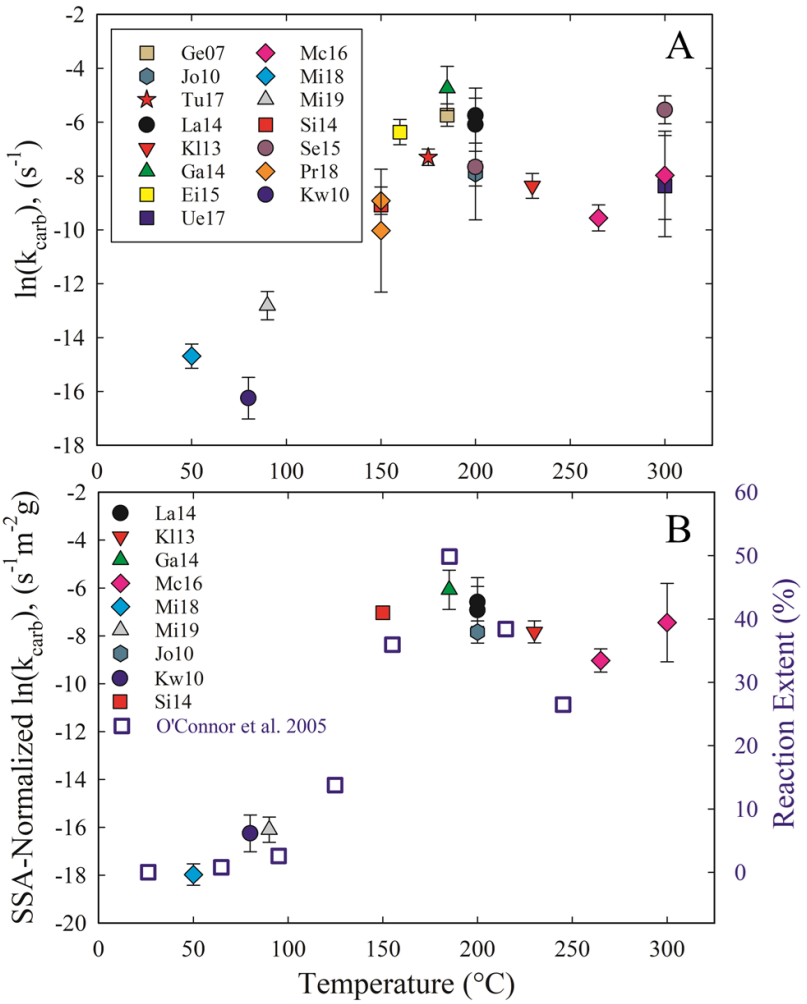

Figure 2. Calculated Avrami rate constants for olivine carbonation datasets [27, 29, 41, 76-85, 87]. Abbreviations correspond to the first two letters of the first author's name and are followed by the last two numbers of the publication year (**Table 1**). The upper panel (a) shows the carbonation rate constants as a function of temperature. The lower panel (b) plots the N_2 BET SSA-normalized rate constants and also includes carbonation reaction extents (open blue squares, right y-axis) from O'Connor et al.[88] for a general reaction trend comparison.

Although progress towards unraveling the associated carbonation and serpentinization pathways and kinetics is ongoing,[77, 80, 106] more investigations are needed to fully constrain the parallel, competitive, and interconnected processes of rock carbonation and serpentinization. In general, we recommend that future mineral reactivity studies include greater sampling density for time-resolved measurements, replicate sample collection, longer reaction times, and improved reactant and product characterization. One barrier to fully realizing the potential of the compiled studies was that nearly half of the studies (**Table 1**) didn't report the initial BET SSA of the reactant olivine, a relatively inexpensive and rapid measurement.

Furthermore, *in situ* experimental techniques to determine the time-resolved abundances of solids (including intermediate phases), gases, fluids, and solutes are required to delineate and quantify carbonation

and serpentinization reactions at elevated pressure and temperature conditions. These techniques are continuing to be developed,[107] as researchers are investigating olivine reactivity at subsurface-relevant conditions with *in situ* optical,[38, 39, 108, 109] nuclear magnetic resonance (NMR),[109-112] and X-ray spectroscopies[113] that complement X-ray scattering and diffraction investigations.[23, 26, 27, 42, 114-116]. Experimental advances need to be partnered with computational studies to help unravel key mechanistic information, such as those that provide insight into processes at olivine-H_2O-CO_2 interfaces[109, 117-123] and the thermodynamic stabilities of Mg-carbonates[124-127]. Coupled reactivity and transport during olivine carbonation is also being evaluated with flow-through[128-130] and diffusion-limited experimental setups[111, 131-134] that simulate a range of realistic fluid-rock ratios, flow rates, and pore network[135, 136] regimes. These studies and others[137-140] are beginning to clarify physicochemical feedbacks between olivine carbonation and porosity-permeability development, including how localized flow rates and crystallographic orientation[141] influence preferential carbonate precipitation. Collectively, these types of studies are vital for ultimately being able to predict the fate and transport of subsurface CO_2 and determining monitoring and verification strategies.

Carbonation in H_2O-saturated CO_2

Two of the low-temperature (<150 °C) studies[27, 29] shown in **Figure 2a** examined carbonation when olivine was exposed to H_2O-saturated $scCO_2$ (wet $scCO_2$), a non-aqueous reactive phase.[142] Dissolution and carbonate precipitation in wet $scCO_2$ is facilitated by the formation of Å- to nm-scale water films on hydrophilic mineral surfaces.[23, 108, 143, 144] Work in this area, including studies of olivine carbonation[23, 26, 27, 29, 94, 109, 112, 143, 145-150], has revealed unique reaction mechanisms and pathways for mineral carbonation that are not attainable in aqueous media. For instance, the properties of Si-rich surface precipitates on carbonating silicates in wet $scCO_2$ are distinct from those that develop in aqueous experiments, and their development is remarkably sensitive to pressure-temperature conditions of the CO_2.[144, 151-153] Also, critical water film thicknesses are required for continuous coupled dissolution-precipitation.[142, 144, 148] Lastly, nucleation and growth of magnesite at low temperatures (~<65 °C) is promoted in wet $scCO_2$[29, 145, 149], likely due to the reduced hydration of Mg^{2+} in nanoscale interfacial water films.[26, 27]

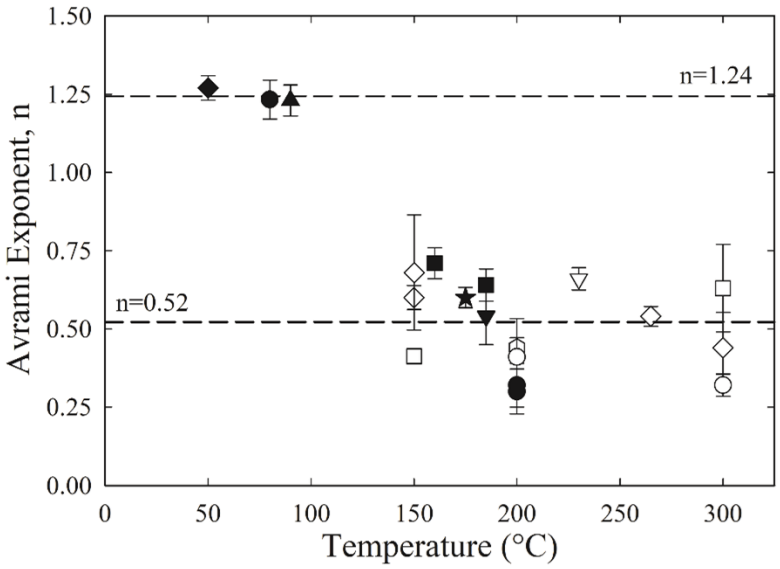

Figure 3. Calculated Avrami exponents, n, for the olivine carbonation datasets [27, 29, 41, 76-85, 87] as a function of temperature. Symbols correspond to the **Figure 2** legend, although the colors distinguish between the **Figure 1a** (black) and **Figure 1b** (white) studies. The reference lines demarcate the average n values for the ≤90 °C and ≥150 °C values.

Despite the large body of initial work, researchers have only managed a glimpse of the reactive potential of wet $scCO_2$. Apart from a basalt carbonation study[154] conducted at 137 °C and 310 bar, relevant studies of the (physico)chemical reactivity of wet $scCO_2$ have been confined to <250 bar and <120 °C (**Figure 4A**). At these conditions, the equilibrium concentration of H_2O in the CO_2 is <3 mol%. At higher temperatures, including those relevant to CO_2-enhanced geothermal systems[155], substantially more H_2O can dissolve into the CO_2-rich fluid, although the exact consequences for reactivity are unclear. For instance, at 250 °C and

500 bar along a prototypical geo-thermal-pressure gradient, the equilibrium concentration of water increases to ~35 mol% (**Figure 4B**); such a dramatic increase would likely lead to enhanced solvation of both inorganic[156, 157] and organic[147] dissolved species. The increased water activity and clustering[158, 159] at elevated temperatures will also likely induce ion formation, which has not yet been detected in wet $scCO_2$.[160] Organic ligands and metal-organic complexes, ubiquitous in diverse geologic settings,[147] can be stable at >200 °C and may contribute to reactions in the bulk CO_2 fluid in addition to those in adsorbed nanoscale water films.[26, 27] These non-aqueous reactions will lead to carbon cycling between organics, carbonate minerals, and CO_2 fluids. It is also unclear how kinetics, thermodynamics, and reaction mechanisms of serpentinization and other metamorphic processes would be influenced by CO_2-dominant fluids. Overall, the expected geochemical properties of H_2O-rich CO_2 and consequences of H_2O-CO_2 phase separation[161, 162] are complex and their potential to induce chemically-driven crustal alteration in natural and engineered settings needs further study.

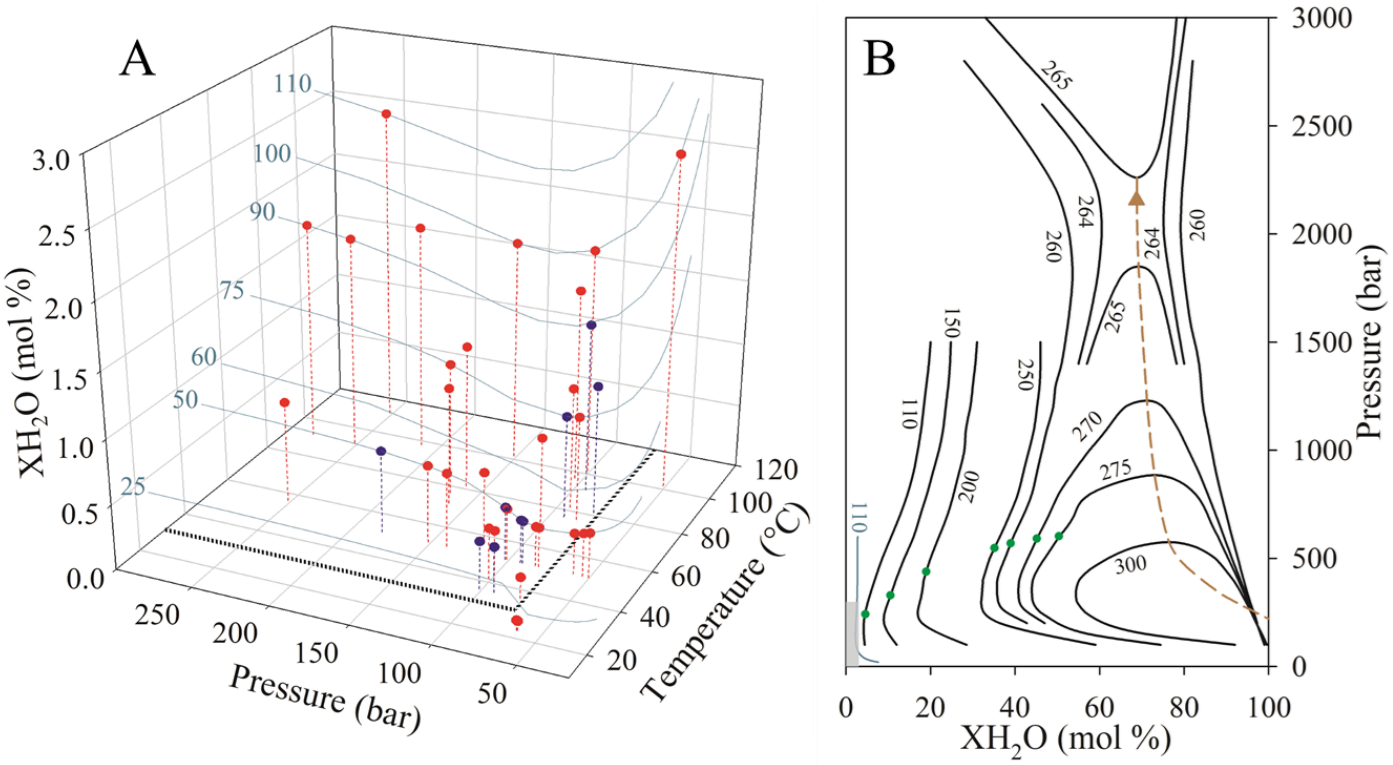

Figure 4. Panel A shows the equilibrium concentration of water (XH_2O) in carbon dioxide as a function of pressure and temperature (P-T). The cyan-colored isotherms are based on the mutual CO_2-H_2O solubility model of Spycher and Pruess[163], and dashed black lines in the P-T plane delineate supercritical CO_2 conditions. Red plotted points denote the P-T conditions of compiled studies[164] that evaluated interactions of minerals, rocks, cement, or steel with water-bearing $scCO_2$. Blue points denote wet $scCO_2$ experiments conducted with olivine [23, 26, 27, 94, 112, 143, 145-150]. Dashed dropdown lines are a visual reference for interpreting the location of the points in three-dimensional space and they illustrate the full range of solubility of water in CO_2 for the specified P-T conditions. Panel B shows phase relationships of CO_2 and H_2O determined experimentally by Takenouchi and Kennedy[165]. The dashed brown curve is the critical curve and the brown triangle marks the minimum critical temperature. The cyan-colored isotherm is based on Spycher and Pruess[163] from Panel A and the light grey field (bottom left) denotes the range of P-XH_2O conditions shown in Panel A. The green circles on the Takenouchi and Kennedy[165] isotherms depict the P-T evolution along a 45 °C/km and 0.435 psi/ft geo-thermal-pressure gradient. General discussions of isotherm placement discrepancies between datasets can be found in Blencoe et al.[166] and Spycher and Pruess[167].

Si-rich Surface Layers

An important aspect that also needs further research is the possible control of grain armoring by emergent surface coatings on the overall rate of Reaction 1. Si-rich passivating layers may develop on olivine by redeposition that limit dissolution and carbonate precipitation.[45, 46, 86, 168-171] Molecular dynamics

simulations[169] of amorphous silica indicate that its inherent permeability should allow for reactants to diffuse through the Si-rich layer, suggesting that the composition of the passivating layer is dynamically complex.[171] Indeed, the Si-rich armoring layers on silicates are more complicated than amorphous silica, and may also include permeability-reducing intergrowths of Fe/Mg/Al-rich phyllosilicates, [44, 86, 171, 172] Fe-oxyhydroxides,[173, 174] hematite,[171, 175] clinohumite,[176] and carbonates.[45, 152] Properties of these armoring phases are spatially complex[168] and vary as a function of reaction time.[168, 172] For example, the temporal evolution of solution redox state to more anoxic conditions during carbonation leads to destabilization of passivating Fe-Si-rich phases.[44, 172, 175] The influences of Fe and redox state on the time-dependent properties of secondary surface layers are exemplified by the prominent 5-day induction time of Sissmann et al.[86] (**Figure 1**, **Table S1**). After the initial phase of the experiment in which no detectable carbonate precipitated, the carbonation trend appeared to conform to Avrami kinetics. The role of Fe in determining the properties of secondary coatings is further supported by studies[26, 27, 29] of Fe-free synthetic forsterite carbonation that didn't result in reaction inhibition, as Fe^{3+}-Si-rich passivating layers were not present. The relationship between fluid redox state and the composition and nm/µm-structure of secondary phases is intriguing in the context of parallel serpentinization and carbonation reactions. An important geologic implication is that reduced fluids containing H_2 (**Reaction 4**) and CH_4 (**Reaction 6**) sourced from serpentinizing systems may promote both carbonation (**Reaction 1**) and hydration (**Reaction 2**) by enabling continuous forsterite dissolution. In one potential redox-front scenario, down-temperature migration of reduced fluids from a serpentinization-dominated regime to shallower depths may enhance carbonation, depending in part on the relative flux of more oxygenated fluids with a surface-associated origin.

Other solutes may influence the development of armoring phases. Sissmann et al.,[86] proposed that dissolution of Al-bearing basalt phases proximal to olivine provides Al that influences the degree of silica polymerization. This hypothesis appears to be consistent with recent results that demonstrate an Al-driven enhancement of olivine dissolution rates.[39, 42, 177] Other fluid compositions also exert a controlling role in determining the properties of secondary coatings, as NaCl and $NaHCO_3$ have been shown to influence the forsterite dissolution and carbonation. In contrast to reactions in ultradilute solutions,[46, 86] the dissolution rate of olivine has been shown to be enhanced by NaCl[45, 81, 170] and significantly promoted by $NaHCO_3$[81], possibly due to inhibition of Si-rich coating development. A follow-up study used NMR spectroscopy to determine that NaCl solutions inhibited the polymerization of amorphous silica.[111]

Overall, the compiled reaction conditions (**Table 1**) suggest that passivating layer development of Sissmann et al.[86] was due to the combination of dilute solutions (i.e. no NaCl, $NaHCO_3$, or NH_3) and Fe-bearing olivine, emphasizing the important nature of these two parameters. Given that most studies included in the present review incorporated agitation (i.e. stirring and rocking, **Table S1**) or carbon-limited fluid compositions, it is challenging to evaluate with certainty how potential reaction passivation trends are related to experimental parameters. Agitation, though necessary to limit diffusion-controlled kinetics, also results in abrasion of surface coatings to expose fresh reactive surfaces. From a technological standpoint, management of carbonation rates via fluid composition may be more cost-effective than mechanical agitation, which is energy-intensive. Nonetheless, it is clear that more systematic work is needed with respect to understanding the impacts of passivation layer development, as the complex properties of Si-rich layers are not only influenced by olivine composition (Fe-content and valence state) and fluid chemistry (i.e. $NaHCO_3$/NaCl concentration[45, 81, 88, 89, 170] and redox state[44, 86, 172, 175]), but by different silicate substrates,[178, 179] specific crystallographic faces,[180] and reaction-induced fracturing/exfoliation.[139, 181-183]

In summary, this review has identified that, across a range of forsterite carbonation studies, rates are optimized at 185-200 °C. It has furthermore shown that the studies are consistent with a carbonation reaction mechanism change at >90 °C, and it has highlighted key knowledge gaps for future research. The

compiled dataset and analysis supports efforts to better understand carbon storage via mineralization and to parametrize reservoir simulators that predict carbonation rates and the carbonation potential of different target reservoirs around the globe. Finally, in addition to supporting the development and deployment of carbon storage technologies in a climate-responding world, reviewing and quantifying olivine reactivity rates in an interpretable, unified, kinetic framework promotes a better understanding how carbonation and serpentinization processes influence critical geochemical cycles[184-186] and other geo-physico-chemical processes[161, 187] on earth and in extraterrestrial environments[188-190].

Author Information

Corresponding Author

* Corresponding Author

Q.R.S. Miller, quinrs.miller@pnnl.gov

Author Contributions

This manuscript was written through contributions of all authors. All authors have given final approval to the final version of the manuscript.

Notes

The authors declare no competing financial interests.

Supporting Information

Tabulated experimental details, notes, and calculated kinetic parameters. This information is available free of charge on the ACS Publications website.

Acknowledgments

This material is based on work supported by the U.S. Department of Energy (DOE), Office of Science, Office of Basic Energy Sciences (BES), Chemical Sciences, Geosciences, and Biosciences Division through its Geosciences program at Pacific Northwest National Laboratory (PNNL). H.T.S. and B.P.M. were supported by the U.S. Department of Energy Office of Fossil Energy at PNNL through the National Energy Technology Laboratory, Morgantown, West Virginia. J.P.K was supported by the University of Wyoming School of Energy Resources and a Nielson Energy Fellowship. We also thank two anonymous reviewers whose insightful and detailed input helped improve the manuscript.

References

1. Newell, P.; Ilgen, A. G., Chapter 1 - Overview of Geological Carbon Storage (GCS). In *Science of Carbon Storage in Deep Saline Formations*, Newell, P.; Ilgen, A. G., Eds. Elsevier: 2018; pp 1-13.

2. Bachu, S.; Gunter, W. D.; Perkins, E. H., Aquifer disposal of CO_2-hydrodynamic and mineral trapping. *Energy Convers. Manage.* **1994,** *35*, 269-274.

3. Kaszuba, J. P.; Janecky, D. R.; Snow, M. G., Carbon dioxide reaction processes in a model brine aquifer at 200 °C and 200 bars: Implications for geologic sequestration of carbon. *Appl. Geochem.* **2003,** *18*, 1065–1080.

4. McGrail, B. P.; Spane, F. A.; Sullivan, E. C.; Bacon, D. H.; Hund, G., The Wallula basalt sequestration pilot project. *Energy Procedia* **2011,** *4*, 5653-5660.

5. McGrail, B. P.; Schaef, H. T.; Ho, A. M.; Chien, Y.-J.; Dooley, J. J.; Davidson, C. L., Potential for carbon dioxide sequestration in flood basalts. *J. Geophys. Res. Solid Earth* **2006,** *111*, B12.

6. Schaef, H. T.; McGrail, B. P.; Owen, A. T., Carbonate mineralization of volcanic province basalts. *Int. J. Greenhouse Gas Control* **2010,** *4*, 249-261.

7. Matter, J. M.; Kelemen, P. B., Permanent storage of carbon dioxide in geological reservoirs by mineral carbonation. *Nat. Geosci.* **2009,** *2*, 837-841.

8. Schaef, H. T.; McGrail, B. P., Dissolution of Columbia River Basalt under mildly acidic conditions as a function of temperature: Experimental results relevant to the geological sequestration of carbon dioxide. *Appl. Geochem.* **2009,** *24*, 980-987.

9. McGrail, B. P.; Schaef, H. T.; Spane, F. A.; Cliff, J. B.; Qafoku, O.; Horner, J. A.; Thompson, C. J.; Owen, A. T.; Sullivan, C. E., Field validation of supercritical CO_2 reactivity with basalts. *Environ. Sci. & Technol. Lett.* **2017,** *4*, 6-10.

10. Matter, J. M.; Stute, M.; Snæbjörnsdottir, S. Ó.; Oelkers, E. H.; Gislason, S. R.; Aradottir, E. S.; Sigfusson, B.; Gunnarsson, I.; Sigurdardottir, H.; Gunnlaugsson, E.; Axelsson, G.; Alfredsson, H. A.; Wolff-Boenisch, D.; Mesfin, K.; Taya, D. F. d. l. R.; Hall, J.; Dideriksen, K.; Broecker, W. S., Rapid carbon mineralization for permanent disposal of anthropogenic carbon dioxide emissions. *Science* **2016,** *352*, 1312-1314.

11. Marieni, C.; Henstock, T. J.; Teagle, D. A., Geological storage of CO_2 within the oceanic crust by gravitational trapping. *Geophys. Res. Lett.* **2013,** *40*, 6219-6224.

12. Goldberg, D. S.; Takahashi, T.; Slagle, A. L., Carbon dioxide sequestration in deep-sea basalt. *PNAS* **2008,** *105*, 9920-9925.

13. Falk, E. S.; Kelemen, P. B., Geochemistry and petrology of listvenite in the Samail ophiolite, Sultanate of Oman: Complete carbonation of peridotite during ophiolite emplacement. *Geochim. Cosmochim. Acta* **2015,** *160*, 70-90.

14. Halls, C.; Zhao, R., Listvenite and related rocks: perspectives on terminology and mineralogy with reference to an occurrence at Cregganbaun, Co. Mayo, Republic of Ireland. *Mineral. Deposita* **1995,** *30*, 303-313.

15. Hansen, L. D.; Dipple, G. M.; Gordon, T. M.; Kellett, D. A., Carbonated serpentinite (listwanite) at Atlin, British Columbia: A geological analogue to carbon dioxide sequestration. *Can. Mineral.* **2005,** *43*, 225-239.

16. Menzel, M. D.; Garrido, C. J.; López Sánchez-Vizcaíno, V.; Marchesi, C.; Hidas, K.; Escayola, M. P.; Delgado Huertas, A., Carbonation of mantle peridotite by CO_2-rich fluids: the formation of listvenites in the Advocate ophiolite complex (Newfoundland, Canada). *Litho* **2018,** *323*, 238-261.

17. Kelemen, P. B.; Matter, J., In situ carbonation of peridotite for CO_2 storage. *PNAS* **2008,** *105*, 17295-17300.

18. Giammar, D. E.; Bruant, R. G.; Peters, C. A., Forsterite dissolution and magnesite precipitation at conditions relevant for deep saline aquifer storage and sequestration of carbon dioxide. *Chem. Geol.* **2005,** *217*, 257-276.

19. Sanna, A.; Hall, M. R.; Maroto-Valer, M., Post-processing pathways in carbon capture and storage by mineral carbonation (CCSM) towards the introduction of carbon neutral materials. *Energy Environ. Sci.* **2012,** *5*, 7781-7796.

20. Gadikota, G., Commentary: Ex Situ Aqueous Mineral Carbonation. *Front. Energy Res.* **2016,** *4*, 21.

21. White, C. E.; Henson, N. J.; Daemen, L. L.; Hartl, M.; Page, K., Uncovering the true atomic structure of disordered materials: The structure of a hydrated amorphous magnesium carbonate ($MgCO_3 \cdot 3D_2O$). *Chem. Mater.* **2014,** *26*, 2693-2702.

22. Hopkinson, L.; Kristova, P.; Rutt, K.; Cressey, G., Phase transitions in the system $MgO\text{-}CO_2\text{-}H_2O$ during CO_2 degassing of Mg-bearing solutions. *Geochim. Cosmochim. Acta* **2012,** *76*, 1-13.

23. Schaef, H. T.; McGrail, B. P.; Loring, J. L.; Bowden, M. E.; Arey, B. W.; Rosso, K. M., Forsterite [Mg_2SiO_4] carbonation in wet supercritical CO_2: An in situ high pressure X-ray diffraction study. *Environ. Sci. Technol.* **2013,** *47*, 174-181.

24. Christ, C. L.; Hostetler, P. B., Studies in the system $MgO\text{-}SiO_2\text{-}CO_2\text{-}H_2O$ (II); the activity-product constant of magnesite. *Am. J. Sci.* **1970,** *268*, 439-453.

25. Lippmann, F., *Sedimentary Carbonate Minerals*. Springer Berlin Heidelberg: Berlin, Heidelberg, 1973; Vol. 6, p 228.

26. Miller, Q. R. S.; Kaszuba, J. P.; Schaef, H. T.; Bowden, M. E.; McGrail, B. P., Impacts of organic ligands on forsterite reactivity in supercritical CO_2 fluids. *Environ. Sci. Technol.* **2015,** *49*, 4724-4734.

27. Miller, Q. R. S.; Schaef, H. T.; Kaszuba, J. P.; Qiu, L.; Bowden, M. E.; McGrail, B. P., Tunable Manipulation of Mineral Carbonation Kinetics in Nanoscale Water Films via Citrate Additives. *Environ. Sci. Technol.* **2018,** *52*, 7138-7148.

28. Power, I. M.; Kenward, P. A.; Dipple, G. M.; Raudsepp, M., Room temperature magnesite precipitation. *Cryst. Growth Des.* **2017,** *17*, 5652-5659.

29. Miller, Q. R. S.; Kaszuba, J. P.; Schaef, H. T.; Bowden, M. E.; McGrail, B. P.; Rosso, K. M., Anomalously low activation energy of nanoconfined $MgCO_3$ precipitation. *Chem. Commun.* **2019,** *55*, 6835-6837.

30. Xu, J.; Yan, C.; Zhang, F. F.; Konishi, H.; Xu, H. F.; Teng, H. H., Testing the cation-hydration effect on the crystallization of $Ca\text{-}Mg\text{-}CO_3$ systems. *PNAS* **2013,** *110*, 17750-17755.

31. Scott, S. R.; Sims, K. W.; Frost, B. R.; Kelemen, P. B.; Evans, K. A.; Swapp, S. M., On the hydration of olivine in ultramafic rocks: Implications from Fe isotopes in serpentinites. *Geochim. Cosmochim. Acta* **2017,** *215*, 105-121.

32. Frost, B. R.; Beard, J. S., On silica activity and serpentinization. *J. Petrol.* **2007,** *48*, 1351-1368.

33. Mayhew, L. E.; Ellison, E. T.; McCollom, T. M.; Trainor, T. P.; Templeton, A. S., Hydrogen generation from low-temperature water-rock reactions. *Nat. Geosci.* **2013,** *6*, 478-484.

34. McCollom, T. M., Miller-Urey and Beyond: What Have We Learned About Prebiotic Organic Synthesis Reactions in the Past 60 Years? *Annu. Rev. Earth Planet. Sci.* **2013,** *41*, 207-229.

35. Rimstidt, J. D.; Brantley, S. L.; Olsen, A. A., Systematic review of forsterite dissolution rate data. *Geochim. Cosmochim. Acta* **2012,** *99*, 159-178.

36. Crundwell, F. K., The mechanism of dissolution of forsterite, olivine and minerals of the orthosilicate group. *Hydrometallurgy* **2014,** *150*, 68-82.

37. Oelkers, E. H.; Declercq, J.; Saldi, G. D.; Gislason, S. R.; Schott, J., Olivine dissolution rates: A critical review. *Chem. Geol.* **2018,** *500*, 1-19.

38. Lamadrid, H. M.; Rimstidt, J. D.; Schwarzenbach, E. M.; Klein, F.; Ulrich, S.; Dolocan, A.; Bodnar, R. J., Effect of water activity on rates of serpentinization of olivine. *Nat. Comm.* **2017,** *8*, 16107.

39. Andreani, M.; Daniel, I.; Pollet-Villard, M., Aluminum speeds up the hydrothermal alteration of olivine. *Am. Mineral.* **2013,** *98*, 1738-1744.

40. Malvoisin, B.; Brunet, F.; Carlut, J.; Roumejon, S.; Cannat, M., Serpentinization of oceanic peridotites: 2. Kinetics and processes of San Carlos olivine hydrothermal alteration. *J. Geophys. Res. Solid Earth* **2012,** *117*, 13.

41. McCollom, T. M.; Klein, F.; Robbins, M.; Moskowitz, B.; Berquo, T. S.; Jons, N.; Bach, W.; Templeton, A., Temperature trends for reaction rates, hydrogen generation, and partitioning of iron during experimental serpentinization of olivine. *Geochim. Cosmochim. Acta* **2016,** *181*, 175-200.

42. Pens, M.; Andreani, M.; Daniel, I.; Perrillat, J.-P.; Cardon, H., Contrasted effect of aluminum on the serpentinization rate of olivine and orthopyroxene under hydrothermal conditions. *Chem. Geol.* **2016,** *441*, 256-264.

43. Saldi, G. D.; Schott, J.; Pokrovsky, O. S.; Gautier, Q.; Oelkers, E. H., An experimental study of magnesite precipitation rates at neutral to alkaline conditions and 100-200 °C as a function of pH, aqueous solution composition and chemical affinity. *Geochim. Cosmochim. Acta* **2012,** *83*, 93-109.

44. Saldi, G. D.; Daval, D.; Morvan, G.; Knauss, K. G., The role of Fe and redox conditions in olivine carbonation rates: An experimental study of the rate limiting reactions at 90 and 150 °C in open and closed systems. *Geochim. Cosmochim. Acta* **2013,** *118*, 157-183.

45. Johnson, N. C.; Thomas, B.; Maher, K.; Rosenbauer, R. J.; Bird, D.; Brown, G. E., Jr., Olivine dissolution and carbonation under conditions relevant for in situ carbon storage. *Chem. Geol.* **2014,** *373*, 93-105.

46. Daval, D.; Sissmann, O.; Menguy, N.; Saldi, G. D.; Guyot, F.; Martinez, I.; Corvisier, J.; Garcia, B.; Machouk, I.; Knauss, K. G.; Hellmann, R., Influence of amorphous silica layer formation on the dissolution rate of olivine at 90 °C and elevated pCO_2. *Chem. Geol.* **2011,** *284*, 193-209.

47. Daval, D., Carbon dioxide sequestration through silicate degradation and carbon mineralisation: promises and uncertainties. *npj Mat. Deg.* **2018,** *2*, 11.

48. Tummer, B. *DataThief III*, 1.7; 2015.

49. Avrami, M., Kinetics of Phase Change. II Transformation-Time Relations for Random Distribution of Nuclei. *J. Chem. Phys.* **1940,** *8*, 212-224.

50. Johnson, W.; Mehl, R., Reaction kinetics in processes of nucleation and growth. *Trans. Am. Inst. Min., Metall. Pet. Eng.* **1939,** *135*, 416-442.

51. Kolmogorov, A. N., On the statistical theory of the crystallization of metals. *Bull. Acad. Sci. USSR, Math. Ser* **1937,** *1*, 355-359.

52. Barmak, K., A Commentary on: "Reaction Kinetics in Processes of Nucleation and Growth". *Metall. Mater. Trans. A* **2010,** *41*, 2711-2775.

53. Perrillat, J. P., Kinetics of high-pressure mineral phase transformations using in situ time-resolved X-ray diffraction in the Paris-Edinburgh cell: A practical guide for data acquisition and treatment. *Min. Mag.* **2008,** *72*, 683-695.

54. Cattaneo, A.; Gualtieri, A.; Artioli, G., Kinetic study of the dehydroxylation of chrysotile asbestos with temperature by in situ XRPD. *Phys. Chem. Miner.* **2003,** *30*, 177-183.

55. Perrillat, J. P.; Daniel, I.; Koga, K. T.; Reynard, B.; Cardon, H.; Crichton, W. A., Kinetics of antigorite dehydration: A real-time X-ray diffraction study. *Earth. Planet. Sci. Lett.* **2005,** *236*, 899-913.

56. Hancock, J. D.; Sharp, J. H., Method of comparing solid-state kinetic data and its application to the decomposition of kaolinite, brucite, and $BaCO_3$. *J. Am. Ceram. Soc.* **1972,** *55*, 74-77.

57. Perrillat, J. P.; Daniel, I.; Lardeaux, J.-M.; Cardon, H., Kinetics of the coesite–quartz transition: Application to the exhumation of ultrahigh-pressure rocks. *J. Petrol.* **2003,** *44*, 773-788.

58. Rimstidt, J. D., *Geochemical Rate Models: An Introduction to Geochemical Kinetics*. Cambridge University Press: 2013.

59. Van Vleet, M. J.; Weng, T.; Li, X.; Schmidt, J. R., In Situ, Time-Resolved, and Mechanistic Studies of Metal–Organic Framework Nucleation and Growth. *Chem. Rev.* **2018,** *118*, 3681-3721.

60. Nikulshina, V.; Gálvez, M. E.; Steinfeld, A., Kinetic analysis of the carbonation reactions for the capture of CO_2 from air via the $Ca(OH)_2$–$CaCO_3$–CaO solar thermochemical cycle. *Chem. Eng. J.* **2007,** *129*, 75-83.

61. Altree-Williams, A.; Pring, A.; Ngothai, Y.; Brugger, J., The Carbonatation of Anhydrite: Kinetics and Reaction Pathways. *ACS Earth and Space Chemistry* **2017,** *1*, 89-100.

62. Scarlett, N. V. Y.; Grey, I. E.; Brand, H. E. A., In situ synchrotron diffraction studies on the formation kinetics of jarosites. *J. Synchrotron Radiat.* **2013,** *20*, 366-375.

63. Wang, H.; Pring, A.; Ngothai, Y.; O'Neill, B., A low-temperature kinetic study of the exsolution of pentlandite from the monosulfide solid solution using a refined Avrami method. *Geochim. Cosmochim. Acta* **2005,** *69*, 415-425.

64. Zhao, J.; Brugger, J.; Pring, A., Mechanism and kinetics of hydrothermal replacement of magnetite by hematite. *Geosci. Front.* **2019,** *10*, 29-41.

65. Xia, F.; Chen, D.; Scarlett, N. V. Y.; Madsen, I. C.; Lau, D.; Leoni, M.; Ilavsky, J.; Brand, H. E. A.; Caruso, R. A., Understanding Solvothermal Crystallization of Mesoporous Anatase Beads by In Situ Synchrotron PXRD and SAXS. *Chem. Mater.* **2014,** *26*, 4563-4571.

66. Pedrosa, E. T.; Boeck, L.; Putnis, C. V.; Putnis, A., The replacement of a carbonate rock by fluorite: Kinetics and microstructure. *Am. Mineral.* **2017,** *102*, 126-134.

67. Di Lorenzo, F.; Rodriguez-Galan, R. M.; Prieto, M., Kinetics of the solvent-mediated transformation of hydromagnesite into magnesite at different temperatures. *Min. Mag.* **2014,** *78*, 1363-1372.

68. Putnis, A., *An Introduction to Mineral Sciences*. Cambridge University Press: 1992.

69. Vu, H. P.; Shaw, S.; Benning, L. G., Transformation of ferrihydrite to hematite: an in situ investigation on the kinetics and mechanisms. *Min. Mag.* **2008,** *72*, 217-220.

70. Spassov, T.; Diakovich, V., A modified Johnson-Mehl-Avrami kinetic model of overall crystallization of Fe-Co-B metallic glasses. *J. Alloys Compd.* **1993,** *198*, 187-191.

71. Croker, D.; Loan, M.; Hodnett, B. K., Kinetics and Mechanisms of the Hydrothermal Crystallization of Calcium Titanate Species. *Cryst. Growth Des.* **2009,** *9*, 2207-2213.

72. Zhou, Y.; Antonova, E.; Bensch, W.; Patzke, G. R., In situ X-ray diffraction study of the hydrothermal crystallization of hierarchical Bi_2WO_6 nanostructures. *Nanoscale* **2010,** *2*, 2412-2417.

73. Finney, E. E.; Finke, R. G., Is There a Minimal Chemical Mechanism Underlying Classical Avrami-Erofe'ev Treatments of Phase-Transformation Kinetic Data? *Chem. Mater.* **2009,** *21*, 4692-4705.

74. Dill, E. D.; Folmer, J. C. W.; Martin, J. D., Crystal Growth Simulations To Establish Physically Relevant Kinetic Parameters from the Empirical Kolmogorov–Johnson–Mehl–Avrami Model. *Chem. Mater.* **2013,** *25*, 3941-3951.

75. Jensen, K. M.; Tyrsted, C.; Bremholm, M.; Iversen, B. B., In situ studies of solvothermal synthesis of energy materials. *ChemSusChem* **2014,** *7*, 1594-1611.

76. Gerdemann, S. J.; O'Connor, W. K.; Dahlin, D. C.; Penner, L. R.; Rush, H., Ex Situ Aqueous Mineral Carbonation. *Environ. Sci. Technol.* **2007,** *41*, 2587-2593.

77. Lafay, R.; Montes-Hernandez, G.; Janots, E.; Chiriac, R.; Findling, N.; Toche, F., Simultaneous precipitation of magnesite and lizardite from hydrothermal alteration of olivine under high-carbonate alkalinity. *Chem. Geol.* **2014,** *368*, 63-75.

78. Jones, L. C.; Rosenbauer, R.; Goldsmith, J. I.; Oze, C., Carbonate control of H_2 and CH_4 production in serpentinization systems at elevated P-Ts. *Geophys. Res. Lett.* **2010,** *37*, L14306.

79. Klein, F.; McCollom, T. M., From serpentinization to carbonation: New insights from a CO_2 injection experiment. *Earth. Planet. Sci. Lett.* **2013,** *379*, 137-145.

80. Přikryl, J.; Stefánsson, A.; Pearce, C. R., Tracing olivine carbonation and serpentinization in CO_2-rich fluids via magnesium exchange and isotopic fractionation. *Geochim. Cosmochim. Acta* **2018,** *243*, 133-148.

81. Gadikota, G.; Matter, J.; Kelemen, P.; Park, A.-h. A., Chemical and morphological changes during olivine carbonation for CO_2 storage in the presence of NaCl and $NaHCO_3$. *PCCP* **2014,** *16*, 4679-4693.

82. Eikeland, E.; Blichfeld, A. B.; Tyrsted, C.; Jensen, A.; Iversen, B. B., Optimized carbonation of magnesium silicate mineral for CO_2 storage. *ACS Appl. Mater. Interfaces* **2015,** *7*, 5258-5264.

83. Ueda, H.; Sawaki, Y.; Maruyama, S., Reactions between olivine and CO_2-rich seawater at 300 °C: Implications for H_2 generation and CO_2 sequestration on the early Earth. *Geosci. Front.* **2017,** *8*, 387-396.

84. Turri, L.; Muhr, H.; Rijnsburger, K.; Knops, P.; Lapicque, F., CO_2 sequestration by high pressure reaction with olivine in a rocking batch autoclave. *Chem. Eng. Sci.* **2017,** *171*, 27-31.

85. Sekine, Y.; Shibuya, T.; Postberg, F.; Hsu, H. W.; Suzuki, K.; Masaki, Y.; Kuwatani, T.; Mori, M.; Hong, P. K.; Yoshizaki, M.; Tachibana, S.; Sirono, S., High-temperature water-rock interactions and hydrothermal environments in the chondrite-like core of Enceladus. *Nat. Comm.* **2015,** *6*, 8604.

86. Sissmann, O.; Brunet, F.; Martinez, I.; Guyot, F.; Verlaguet, A.; Pinquier, Y.; Daval, D., Enhanced Olivine Carbonation within a Basalt as Compared to Single-Phase Experiments: Reevaluating the Potential of CO_2 Mineral Sequestration. *Environ. Sci. Technol.* **2014,** *48*, 5512-5519.

87. Kwak, J. H.; Hu, J. Z.; Hoyt, D. W.; Sears, J. A.; Wang, C.; Rosso, K. M.; Felmy, A. R., Metal carbonation of forsterite in supercritical CO_2 and H_2O using solid state ^{29}Si, ^{13}C NMR spectroscopy. *J. Phys. Chem. C* **2010,** *114*, 4126-4134.

88. O'Connor, W.; Dahlin, D.; Rush, G.; Gerdemann, S.; Penner, L.; Nilsen, D. *Aqueous mineral carbonation: Mineral availability, pretreatment, reaction parametrics, and process studies (DOE/ARC-TR-04-002)*; National Energy Technology Laboratory: Albany, OR, USA, 2005.

89. Gerdemann, S.; Dahlin, D.; O'Connor, W.; Penner, L. *Carbon dioxide sequestration by aqueous mineral carbonation of magnesium silicate minerals (DOE/ARC-2003-018)*; National Energy Technology Laboratory: Albany, OR, USA, 2003.

90. Chizmeshya, A. V.; McKelvy, M. J.; Squires, K.; Carpenter, R. W.; Bearat, H. *A novel approach to mineral carbonation: Enhancing carbonation while avoiding mineral pretreatment process cost*; Arizona State Univ., Tempe, AZ (United States): 2007.

91. Kularatne, K.; Sissmann, O.; Kohler, E.; Chardin, M.; Noirez, S.; Martinez, I., Simultaneous ex-situ CO_2 mineral sequestration and hydrogen production from olivine-bearing mine tailings. *Appl. Geochem.* **2018,** *95*, 195-205.

92. Dufaud, F.; Martinez, I.; Shilobreeva, S., Experimental study of Mg-rich silicates carbonation at 400 and 500 °C and 1 kbar. *Chem. Geol.* **2009,** *265*, 79-87.

93. Bischoff, J. L.; Rosenbauer, R. J., The alteration of rhyolite in CO_2 charged water at 200 and 350°C: The unreactivity of CO_2 at higher temperature. *Geochim. Cosmochim. Acta* **1996,** *60*, 3859-3867.

94. Lacinska, A. M.; Styles, M. T.; Bateman, K.; Hall, M.; Brown, P., An experimental study of the carbonation of serpentinite and partially serpentinised peridotites. *Front. Earth. Sci.* **2017,** *5*, 37.

95. Grozeva, N. G.; Klein, F.; Seewald, J. S.; Sylva, S. P., Experimental study of carbonate formation in oceanic peridotite. *Geochim. Cosmochim. Acta* **2017,** *199*, 264-286.

96. Galvez, M. E.; Beyssac, O.; Martinez, I.; Benzerara, K.; Chaduteau, C.; Malvoisin, B.; Malavieille, J., Graphite formation by carbonate reduction during subduction. *Nat. Geosci.* **2013,** *6*, 473-477.

97. McCollom, T. M.; Seewald, J. S., A reassessment of the potential for reduction of dissolved CO_2 to hydrocarbons during serpentinization of olivine. *Geochim. Cosmochim. Acta* **2001,** *65*, 3769-3778.

98. Neubeck, A.; Nguyen, D. T.; Etiope, G., Low-temperature dunite hydration: evaluating CH_4 and H_2 production from H_2O and CO_2. *Geofluids* **2016,** *16*, 408-420.

99. Zandanel, A.; Truche, L.; Hellmann, R.; Tobie, G.; Marrocchi, Y. In *Dissolution Rates and Reaction Products of Olivine Interaction with Ammonia-Rich Fluid*, Ocean Worlds 2018.

100. Saldi, G. D.; Jordan, G.; Schott, J.; Oelkers, E. H., Magnesite growth rates as a function of temperature and saturation state. *Geochim. Cosmochim. Acta* **2009,** *73*, 5646-5657.

101. Lüttge, A., Crystal dissolution kinetics and Gibbs free energy. *J. Electron. Spectrosc. Relat. Phenom.* **2006,** *150*, 248-259.

102. Yan, J., Negative-emissions hydrogen energy. *Nat. Clim. Change* **2018,** *8*, 560-561.

103. Malvoisin, B.; Brunet, F.; Carlut, J.; Montes-Hernandez, G.; Findling, N.; Lanson, M.; Vidal, O.; Bottero, J.-Y.; Goffe, B., High-purity hydrogen gas from the reaction between BOF steel slag and water in the 473–673 K range. *Int. J. Hydrogen Energy* **2013,** *38*, 7382-7393.

104. Martin, B.; Fyfe, W., Some experimental and theoretical observations on the kinetics of hydration reactions with particular reference to serpentinization. *Chem. Geol.* **1970,** *6*, 185-202.

105. Wegner, W. W.; Ernst, W., Experimentally determined hydration and dehydration reaction rates in the system MgO-SiO_2-H_2O. *Am. J. Sci.* **1983,** *283*, 151-180.

106. Fritz, B.; Clément, A.; Montes-Hernandez, G.; Noguera, C., Theoretical analysis of the kinetics of precipitation of lizardite and magnesite from olivine alteration. *Chem. Geol.* **2018,** *497*, 18-26.

107. Kaszuba, J.; Yardley, B.; Andreani, M., Experimental perspectives of mineral dissolution and precipitation due to carbon dioxide-water-rock interactions. In *Geochemistry of Geologic CO_2 Sequestration*, DePaolo, D. J.; Cole, D. R.; Navrotsky, A.; Bourg, I. C., Eds. The Mineralogical Society of America: Chantilly, Virginia, 2013; Vol. 77, pp 153-188.

108. Loring, J. S.; Miller, Q. R. S.; Schaef, H. T.; Thompson, C. J., Experimental studies of reactivity and transformations of rocks and minerals in water-bearing supercritical CO_2. In *Science of Carbon Storage in Deep Saline Formations: Process Coupling across Time and Spatial Scales*, 1st ed.; Newell, P.; Ilgen, A. G., Eds. Elsevier: 2018.

109. Miller, Q. R. S.; Dixon, D. A.; Burton, S. D.; Walter, E. D.; Hoyt, D. W.; McNeill, A. S.; Moon, J. D.; Thanthiriwatte, K. S.; Ilton, E. S.; Qafoku, O.; Thompson, C. J.; Schaef, H. T.; Rosso, K. M.; Loring, J. S., Surface-Catalyzed Oxygen Exchange during Mineral Carbonation in Nanoscale Water Films. *J. Phys. Chem. C* **2019,** *123*, 12871-12885.

110. Sesti, E. L.; Cui, J.; Hayes, S. E.; Conradi, M. S., A flow-through, elevated-temperature and-pressure NMR apparatus for in-situ CO_2 sequestration studies. *J. Magn. Reson.* **2017,** *282*, 136-141.

111. Cui, J. L.; Sesti, E. L.; Moore, J. K.; Giammar, D. E.; Hayes, S. E., Evidence from ^{29}Si Solid-State Nuclear Magnetic Resonance of Dissolution Reactions of Forsterite. *Environ. Eng. Sci.* **2016,** *33*, 799-805.

112. Kwak, J. H.; Hu, J. Z.; Turcu, R. V. F.; Rosso, K. M.; Ilton, E. S.; Wang, C.; Sears, J. A.; Engelhard, M. H.; Felmy, A. R.; Hoyt, D. W., The role of H_2O in the carbonation of forsterite in supercritical CO_2. *Int. J. Greenhouse Gas Control* **2011,** *5*, 1081-1092.

113. Daval, D.; Testemale, D.; Recham, N.; Tarascon, J.-M.; Siebert, J.; Martinez, I.; Guyot, F., Fayalite (Fe_2SiO_4) dissolution kinetics determined by X-ray absorption spectroscopy. *Chem. Geol.* **2010,** *275*, 161-175.

114. Wolf, G. H.; Chizmeshya, A. V. G.; Diefenbacher, J.; McKelvy, M. J., In situ observation of CO_2 sequestration reactions using a novel microreaction system. *Environ. Sci. Technol.* **2004,** *38*, 932-936.

115. Gadikota, G., Multiscale X-Ray Scattering for Probing Chemo-Morphological Coupling in Pore-to-Field and Process Scale Energy and Environmental Applications. In *Small Angle Scattering and Diffraction*, IntechOpen: 2018.

116. Yan, H. P.; Park, C.; Ahn, G.; Hong, S.; Keane, D. T.; Kenney-Benson, C.; Chow, P.; Xiao, Y. M.; Shen, G. Y., Termination and hydration of forsteritic olivine (010) surface. *Geochim. Cosmochim. Acta* **2014,** *145*, 268-280.

117. Kerisit, S.; Bylaska, E. J.; Felmy, A., Water and carbon dioxide adsorption at olivine surfaces. *Chem. Geol.* **2013,** *359*, 81-89.

118. Kerisit, S.; Weare, J. H.; Felmy, A. R., Structure and dynamics of forsterite-scCO_2/H_2O interfaces as a function of water content. *Geochim. Cosmochim. Acta* **2012,** *84*, 137-151.

119. Liu, T.; Gautam, S.; Wang, H.-W.; Anovitz, L. M.; Mamontov, E.; Allard, L. F.; Cole, D. R., Structure and Dynamics of Water on Forsterite Surface. *PCCP* **2018,** *20*, 27822--27829.

120. Morrow, C. P.; Olsen, A. A.; Kubicki, J. D., Quantum mechanical modeling of hydrolysis and H_2O-exchange in Mg-, Ca-, and Ni- silicate clusters: Implications for dissolution mechanisms of olivine minerals. *Am. Mineral.* **2014,** *99*, 2303-2312.

121. Prigiobbe, V.; Negreira, A. S.; Wilcox, J., Interaction between Olivine and Water Based on Density Functional Theory Calculations. *J. Phys. Chem. C* **2013,** *117*, 21203-21216.

122. Liu, T.; Luo, W.; Cole, D. R.; Asthagiri, A., Water adsorption on olivine (010) surfaces: Effect of alkali and transition metal cation doping. *J. Chem. Phys.* **2019,** *150*, 044703.

123. Escamilla-Roa, E.; Martin-Torres, J.; Sainz-Díaz, C. I., Adsorption of methane and CO_2 onto olivine surfaces in Martian dust conditions. *Planet. Space Sci.* **2018,** *153*, 163-171.

124. Chaka, A. M., Ab Initio Thermodynamics and the Relationship between Octahedral Distortion, Lattice Structure, and Proton Substitution Defects in Malachite/Rosasite Group Endmember Pokrovskite $Mg_2CO_3(OH)_2$. *J. Phys. Chem. A* **2016,** *120*, 10181-10195.

125. Chaka, A. M.; Felmy, A. R., Ab initio thermodynamic model for magnesium carbonates and hydrates. *J. Phys. Chem. A* **2014,** *118*, 7469-7488.

126. Chaka, A. M.; Felmy, A. R.; Qafoku, O., Ab initio thermodynamics of magnesium carbonates and hydrates in water-saturated supercritical CO_2 and CO_2-rich regions. *Chem. Geol.* **2016,** *434*, 1-11.

127. Chaka, A. M., Quantifying the Impact of Magnesium on the Stability and Water Binding Energy of Hydrated Calcium Carbonates by Ab Initio Thermodynamics. *J. Phys. Chem. A* **2019,** *123*, 2908-2923.

128. Andreani, M.; Luquot, L.; Gouze, P.; Godard, M.; Hoise, E.; Gibert, B., Experimental Study of Carbon Sequestration Reactions Controlled by the Percolation of CO_2-Rich Brine through Peridotites. *Environ. Sci. Technol.* **2009,** *43*, 1226-1231.

129. Peuble, S.; Godard, M.; Luquot, L.; Andreani, M.; Martinez, I.; Gouze, P., CO_2 geological storage in olivine rich basaltic aquifers: New insights from reactive-percolation experiments. *Appl. Geochem.* **2015,** *52*, 174-190.

130. Peuble, S.; Andreani, M.; Gouze, P.; Pollet-Villard, M.; Reynard, B.; Van de Moortele, B., Multi-scale characterization of the incipient carbonation of peridotite. *Chem. Geol.* **2018,** *476*, 150-160.

131. Giammar, D. E.; Wang, F.; Guo, B.; Surface, J. A.; Peters, C. A.; Conradi, M. S.; Hayes, S. E., Impacts of Diffusive Transport on Carbonate Mineral Formation from Magnesium Silicate-CO_2-Water Reactions. *Environ. Sci. Technol.* **2014,** *48*, 14344-14351.

132. Xiong, W.; Wells, R. K.; Giammar, D. E., Carbon Sequestration in Olivine and Basalt Powder Packed Beds. *Environ. Sci. Technol.* **2017,** *51*, 2105-2112.

133. Wells, R. K.; Xiong, W.; Sesti, E.; Cui, J.; Giammar, D.; Skemer, P.; Hayes, S. E.; Conradi, M. S., Spatially-variable carbonation reactions in polycrystalline olivine. *Geochim. Cosmochim. Acta* **2017,** *204*, 252-266.

134. Xiong, W.; Giammar, D., Forsterite Carbonation in Zones with Transport Limited by Diffusion. *Environ. Sci. & Technol. Lett.* **2014,** *1*, 333-338.

135. Tutolo, B. M.; Mildner, D. F. R.; Gagnon, C. V. L.; Saar, M. O.; Seyfried, W. E., Nanoscale constraints on porosity generation and fluid flow during serpentinization. *Geology* **2016,** *44*, 103-106.

136. Luhmann, A. J.; Tutolo, B. M.; Bagley, B. C.; Mildner, D. F. R.; Scheuermann, P. P.; Feinberg, J. M.; Ignatyev, K.; Seyfried, W. E., Chemical and physical changes during seawater flow through intact dunite cores: An experimental study at 150–200 °C. *Geochim. Cosmochim. Acta* **2017,** *214*, 86-114.

137. Lisabeth, H. P.; Zhu, W.; Kelemen, P. B.; Ilgen, A., Experimental evidence for chemo-mechanical coupling during carbon mineralization in ultramafic rocks. *Earth. Planet. Sci. Lett.* **2017,** *474*, 355-367.

138. Xing, T.; Zhu, W.; Fusseis, F.; Lisabeth, H., Generating porosity during olivine carbonation via dissolution channels and expansion cracks. *Solid Earth* **2018,** *9*, 879–896.

139. Zhu, W.; Fusseis, F.; Lisabeth, H.; Xing, T.; Xiao, X.; De Andrade, V.; Karato, S. i., Experimental evidence of reaction-induced fracturing during olivine carbonation. *Geophys. Res. Lett.* **2016,** *43*, 9535-9543.

140. Lafay, R.; Montes-Hernandez, G.; Renard, F.; Vonlanthen, P., Intracrystalline Reaction-Induced Cracking in Olivine Evidenced by Hydration and Carbonation Experiments. *Minerals* **2018,** *8*, 412.

141. Peuble, S.; Andreani, M.; Godard, M.; Gouze, P.; Barou, F.; Van de Moortele, B.; Mainprice, D.; Reynard, B., Carbonate mineralization in percolated olivine aggregates: Linking effects of crystallographic orientation and fluid flow. *Am. Mineral.* **2015,** *100*, 474-482.

142. McGrail, B. P.; Schaef, H. T.; Glezakou, V. A.; Dang, L. X.; Owen, A. T., Water reactivity in the liquid and supercritical CO_2 phase: Has half the story been neglected? *Energy Procedia* **2009,** *1*, 3415-3419.

143. Loring, J. S.; Thompson, C. J.; Wang, Z.; Joly, A. G.; Sklarew, D. S.; Schaef, H. T.; Ilton, E. S.; Rosso, K. M.; Felmy, A. R., In situ infrared spectroscopic study of forsterite carbonation in wet supercritical CO_2. *Environmental Science & Technology* **2011,** *45*, 6204-6210.

144. Miller, Q. R. S.; Thompson, C. J.; Loring, J. S.; Windisch, C. F.; Bowden, M. E.; Hoyt, D. W.; Hu, J. Z.; Arey, B. W.; Rosso, K. M.; Schaef, H. T., Insights into silicate carbonation processes in water-bearing supercritical CO_2 fluids. *International Journal of Greenhouse Gas Control* **2013,** *15*, 104-118.

145. Felmy, A. R.; Qafoku, O.; Arey, B. W.; Hu, J. Z.; Hu, M.; Schaef, H. T.; Ilton, E. S.; Hess, N. J.; Pearce, C. I.; Feng, J.; Rosso, K. M., Reaction of water-saturated supercritical CO_2 with forsterite: Evidence for magnesite formation at low temperatures. *Geochim. Cosmochim. Acta* **2012,** *91*, 271-282.

146. Thompson, C. J.; Loring, J. S.; Rosso, K. M.; Wang, Z., Comparative reactivity study of forsterite and antigorite in wet supercritical CO_2 by in situ infrared spectroscopy. *Int. J. Greenhouse Gas Control* **2013,** *18*, 246-255.

147. Miller, Q. R. S.; Kaszuba, J. P.; Schaef, H. T.; Thompson, C. J.; Qiu, L.; Bowden, M. E.; Glezakou, V. A.; McGrail, B. P., Experimental study of organic ligand transport in supercritical CO_2 fluids and impacts to silicate reactivity. *Energy Procedia* **2014,** *63*, 3225-3233.

148. Loring, J. S.; Chen, J.; Benezeth, P.; Qafoku, O.; Ilton, E. S.; Washton, N. M.; Thompson, C. J.; Martin, P. F.; McGrail, B. P.; Rosso, K. M.; Felmy, A. R.; Schaef, H. T., Evidence for carbonate surface complexation during forsterite carbonation in wet supercritical carbon dioxide. *Langmuir* **2015,** *31*, 7533-7543.

149. Qafoku, O.; Hu, J.; Hess, N. J.; Hu, M. Y.; Ilton, E. S.; Feng, J.; Arey, B. W.; Felmy, A. R., Formation of submicron magnesite during reaction of natural forsterite in H_2O-saturated supercritical CO_2. *Geochim. Cosmochim. Acta* **2014,** *134*, 197-209.

150. Schaef, H. T.; Miller, Q. R. S.; Thompson, C. J.; Loring, J. S.; Bowden, M. S.; Arey, B. W.; McGrail, B. P.; Rosso, K. M., Silicate carbonation in supercritical CO_2 containing dissolved H_2O: An in situ high pressure X-ray diffraction and infrared spectroscopy study. *Energy Procedia* **2013,** *37*, 5892-5896.

151. Whitfield, P. S.; Mitchell, L. D., In situ laboratory X-ray powder diffraction study of wollastonite carbonation using a high-pressure stage. *Appl. Geochem.* **2009,** *24*, 1635-1639.

152. Daval, D.; Martinez, I.; Guigner, J.-M.; Hellmann, R.; Corvisier, J.; Findling, N.; Dominici, C.; Goffe, B.; Guyot, F., Mechanism of wollastonite carbonation deduced from micro- to nanometer length scale observations. *Am. Mineral.* **2009,** *94*, 1707-1726.

153. Min, Y.; Li, Q.; Voltolini, M.; Kneafsey, T.; Jun, Y.-S., Wollastonite Carbonation in Water-Bearing Supercritical CO_2: Effects of Particle Size. *Environ. Sci. Technol.* **2017,** *51*, 13044-13053.

154. Schaef, H. T.; McGrail, B. P.; Owen, A. T., Basalt reactivity variability with reservoir depth in supercritical CO_2 and aqueous phases. *Energy Procedia* **2011,** *4*, 4977-4984.

155. Lo Ré, C.; Kaszuba, J. P.; Moore, J. N.; McPherson, B. J., Fluid-rock interactions in CO_2-saturated, granite-hosted geothermal systems: Implications for natural and engineered systems from geochemical experiments and models. *Geochim. Cosmochim. Acta* **2014,** *141*, 160-178.

156. Rempel, K. U.; Liebscher, A.; Heinrich, W.; Schettler, G., An experimental investigation of trace element dissolution in carbon dioxide: Applications to the geological storage of CO_2. *Chem. Geol.* **2011,** *289*, 224-234.

157. Garrels, R. M.; Richter, D. H., Is carbon dioxide an ore-forming fluid under shallow-earth conditions? *Econ. Geol.* **1955,** *50*, 447-457.

158. Oparin, R.; Tassaing, T.; Danten, Y.; Besnard, M., A vibrational spectroscopic study of structure evolution of water dissolved in supercritical carbon dioxide under isobaric heating. *J. Chem. Phys.* **2004,** *120*, 10691-10698.

159. Oparin, R.; Tassaing, T.; Danten, Y.; Besnard, M., Water-carbon dioxide mixtures at high temperatures and pressures: Local order in the water rich phase investigated by vibrational spectroscopy. *J. Chem. Phys.* **2005,** *123*, 224501.

160. Capobianco, R. M.; Gruszkiewicz, M. S.; Bodnar, R. J.; Rimstidt, J. D., Conductivity Measurements on H_2O-Bearing CO_2-Rich Fluids. *J. Solution Chem.* **2015,** *44*, 934-962.

161. Kaszuba, J. P.; Williams, L. L.; Janecky, D. R.; Hollis, W. K.; Tsimpanogiannis, I. N., Immiscible CO_2-H_2O fluids in the shallow crust. *Geochem. Geophys. Geosyst.* **2006,** *7(10)*, Q10003.

162. Heinrich, W., Fluid immiscibility in metamorphic rocks. In *Reviews in Mineralogy and Geochemistry: Fluid-Fluid Interactions*, Mineralogical Society of America: 2007; Vol. 65, pp 389-430.

163. Spycher, N.; Pruess, K., CO_2-H_2O mixtures in the geological sequestration of CO_2. II. Partitioning in chloride brines at 12-100 °C and up to 600 bar. *Geochim. Cosmochim. Acta* **2005,** *69*, 3309-3320.

164. Miller, Q. R. S. Geochemistry of multiphase CO_2-H_2O-rock interactions in nanoconfined environments. PhD Dissertation, University of Wyoming, Laramie, WY, August, 2017.

165. Takenouchi, S.; Kennedy, G. C., Binary system H_2O-CO_2 at high temperatures and pressures. *Am. J. Sci.* **1964,** *262*, 1055-1074.

166. Blencoe, J. G.; Naney, M. T.; Anovitz, L. M., The CO_2-H_2O system: III. A new experimental method for determining liquid-vapor equilibria at high subcritical temperatures. *Am. Mineral.* **2001,** *86*, 1100-1111.

167. Spycher, N.; Pruess, K., A Phase-Partitioning Model for CO_2-Brine Mixtures at Elevated Temperatures and Pressures: Application to CO_2-Enhanced Geothermal Systems. *Transport Porous Med.* **2010,** *82*, 173-196.

168. Maher, K.; Johnson, N. C.; Jackson, A.; Lammers, L. N.; Torchinsky, A. B.; Weaver, K. L.; Bird, D. K.; Brown, G. E., Jr., A spatially resolved surface kinetic model for forsterite dissolution. *Geochim. Cosmochim. Acta* **2016,** *174*, 313-334.

169. Bearat, H.; McKelvy, M. J.; Chizmeshya, A. V. G.; Gormley, D.; Nunez, R.; Carpenter, R. W.; Squires, K.; Wolf, G. H., Carbon sequestration via aqueous olivine mineral carbonation: Role of passivating layer formation. *Environ. Sci. Technol.* **2006,** *40*, 4802-4808.

170. Wang, F.; Giammar, D. E., Forsterite Dissolution in Saline Water at Elevated Temperature and High CO_2 Pressure *Environ. Sci. Technol.* **2013,** *47*, 168-173.

171. King, H. E.; Plumper, O.; Putnis, A., Effect of Secondary Phase Formation on the Carbonation of Olivine. *Environ. Sci. Technol.* **2010,** *44*, 6503-6509.

172. Sissmann, O.; Daval, D.; Brunet, F.; Guyot, F.; Verlaguet, A.; Pinquier, Y.; Findling, N.; Martinez, I., The deleterious effect of secondary phases on olivine carbonation yield: Insight from time-resolved aqueous-fluid sampling and FIB-TEM characterization. *Chem. Geol.* **2013,** *357*, 186-202.

173. Jones, C. L.; Brearley, A. J., Experimental aqueous alteration of the Allende meteorite under oxidizing conditions: Constraints on asteroidal alteration. *Geochim. Cosmochim. Acta* **2006,** *70*, 1040-1058.

174. Smith, K. L.; Milnes, A. R.; Eggleton, R. A., Weathering of basalt: formation of iddingsite. *Clays Clay Miner.* **1987,** *35*, 418-428.

175. Saldi, G. D.; Daval, D.; Guo, H.; Guyot, F.; Bernard, S.; Le Guillou, C.; Davis, J. A.; Knauss, K. G., Mineralogical evolution of Fe-Si-rich layers at the olivine-water interface during carbonation reactions. *Am. Mineral.* **2015,** *100*, 2655-2669.

176. Davis, M. C.; Brouwer, W. J.; Wesolowski, D. J.; Anovitz, L. M.; Lipton, A. S.; Mueller, K. T., Magnesium silicate dissolution investigated by ^{29}Si MAS, ^{1}H-^{29}Si CPMAS, ^{25}Mg QCPMG, and ^{1}H-^{25}Mg CP QCPMG NMR. *PCCP* **2009,** *11*, 7013-7021.

177. Huang, R.; Song, M.; Ding, X.; Zhu, S.; Zhan, W.; Sun, W., Influence of pyroxene and spinel on the kinetics of peridotite serpentinization. *J. Geophys. Res. Solid Earth* **2017,** *122*, 7111-7126.

178. Daval, D., Sissmann, O., Corvisier, J., Garcia, B., Martinez, I., Guyot, F., Hellmann, R. In *The effect of silica coatings on the weathering rates of wollastonite ($CaSiO_3$) and forsterite (Mg_2SiO_4): An apparent paradox?*, In *Water Rock Interaction*, 2010; Birkle, P.; Torres-Alvarado, I. S., Eds. Taylor & Francis Group: 2010; pp 713-716.

179. Hellmann, R.; Wirth, R.; Daval, D.; Barnes, J. P.; Penisson, J. M.; Tisserand, D.; Epicier, T.; Florin, B.; Hervig, R. L., Unifying natural and laboratory chemical weathering with interfacial dissolution-reprecipitation: A study based on the nanometer-scale chemistry of fluid-silicate interfaces. *Chem. Geol.* **2012,** *294*, 203-216.

180. Daval, D.; Bernard, S.; Remusat, L.; Wild, B.; Guyot, F.; Micha, J. S.; Rieutord, F.; Magnin, V.; Fernandez-Martinez, A., Dynamics of altered surface layer formation on dissolving silicates. *Geochim. Cosmochim. Acta* **2017,** *209*, 51-69.

181. Plumper, O.; Royne, A.; Magraso, A.; Jamtveit, B., The interface-scale mechanism of reaction-induced fracturing during serpentinization. *Geology* **2012,** *40*, 1103-1106.

182. Hovelmann, J.; Austrheim, H.; Jamtveit, B., Microstructure and porosity evolution during experimental carbonation of a natural peridotite. *Chem. Geol.* **2012,** *334*, 254-265.

183. Jarvis, K.; Carpenter, R. W.; Windman, T.; Kim, Y.; Nunez, R.; Alawneh, F., Reaction Mechanisms for Enhancing Mineral Sequestration of CO_2. *Environ. Sci. Technol.* **2009,** *43*, 6314-6319.

184. Stevens, T. O.; McKinley, J. P., Abiotic controls on H_2 production from basalt-water reactions and implications for aquifer biogeochemistry. *Environ. Sci. Technol.* **2000,** *34*, 826-831.

185. Dessert, C.; Dupre, B.; Gaillardet, J.; Francois, L. M.; Allegre, C. J., Basalt weathering laws and the impact of basalt weathering on the global carbon cycle. *Chem. Geol.* **2003,** *202*, 257-273.

186. Früh-Green, G. L.; Connolly, J. A. D.; Plas, A.; Kelley, D. S.; Grobéty, B., Serpentinization of oceanic peridotites: Implications for geochemical cycles and biological activity. In *The Subseafloor Biosphere at Mid-Ocean Ridges*, Wilcock, W. S. D.; DeLong, E. F.; Kelley, D. S.; Baross, J. A.; Cary, S. C., Eds. 2004; Vol. 144, pp 119-136.

187. Janecky, D. R.; Seyfried, W. E., Hydrothermal serpentinization of peridotite within the oceanic-crust: Experimental investigations of mineralogy and major element chemistry. *Geochim. Cosmochim. Acta* **1986,** *50*, 1357-1378.

188. Schulte, M.; Blake, D.; Hoehler, T.; McCollom, T., Serpentinization and its implications for life on the early Earth and Mars. *Astrobiology* **2006,** *6*, 364-376.

189. Waite, J. H.; Glein, C. R.; Perryman, R. S.; Teolis, B. D.; Magee, B. A.; Miller, G.; Grimes, J.; Perry, M. E.; Miller, K. E.; Bouquet, A.; Lunine, J. I.; Brockwell, T.; Bolton, S. J., Cassini finds molecular hydrogen in the Enceladus plume: Evidence for hydrothermal processes. *Science* **2017,** *356*, 155.

190. Milliken, R. E.; Rivkin, A. S., Brucite and carbonate assemblages from altered olivine-rich materials on Ceres. *Nat. Geosci.* **2009,** *2*, 258.

TOC Artwork